SCIENCE CHINA
Technological Sciences

• Article •

October 2019 Vol. 62 No. 10: 1845–1853
https://doi.org10.1007/s11431-018-9377-8

A new control design for a morphing UAV based on disturbance observer and command filtered backstepping techniques

WU KeJian[1*], ZHANG PeiXi[2] & WU Hao[3]

[1]*School of Instrumentation Science and Opto-Electronics Engineering, Beihang University, Beijing 100191, China;*
[2]*The 9th Designing of China Aerospace Science Industry Corporation, Wuhan 430040, China;*
[3]*School of Automation Science and Electrical Engineering, Beihang University, Beijing 100191, China*

Received July 12, 2018; accepted October 17, 2018; published online June 27, 2019

Morphing unmanned aerial vehicle (UAV) can manipulate its shape for excellent flight performance under different conditions. The most research of the morphing UAV focuses on modeling. However, the issues including nonlinear characteristics, strong couplings, and mismatched disturbances are inevitable, which can lead to a great challenge in controller design. In this paper, a composite anti-disturbance controller is developed for morphing UAV to achieve enhanced flight performance under multiple sources of disturbances. In the inner loop, a nonlinear disturbance observer (DO) is constructed to estimate the inertial forces and moment; while in the outer loop, the command filtered backstepping (CFBS) method is adopted to guarantee the stability of the closed-loop system. The system outputs can promptly track reference signals in the morphing process of the UAV. The novelty is that the disturbance estimations are added into the control laws to compensate the mismatched disturbances. When comparing to the previous methods, the control scheme presented in this study can significantly improve the performance of anti-disturbance. Finally, the effectiveness of the proposed method is illustrated by numerical simulations.

morphing UAV, longitudinal altitude, disturbance observer, command filtered backstepping

Citation: Wu K J, Zhang P X, Wu H. A new control design for a morphing UAV based on disturbance observer and command filtered backstepping techniques. Sci China Tech Sci, 2019, 62: 1845–1853, https://doi.org/10.1007/s11431-018-9377-8

1 Introduction

The increasing demands of reliability and maneuverability have motivated the development of morphing UAVs [1, 2]. This type of UAVs can alter the shape in response to different flight conditions using variable span, variable sweep, and folding wings. Morphing UAVs, which have potential of accomplishing multi-tasks, have drawn considerable attention [3–5], especially on the aspects of modeling and control of morphing UAVs.

The modeling or control problem for conventional aircrafts has been extensively studied. The research of anti-disturbance control problem can be shown in the following papers. A nonlinear disturbance observer (DO) based command filter backstepping (CFBS) control method is proposed for a missile system in the presence of multiple disturbances [6]. The CFBS method is adopted to achieve trajectory tracking of a small-scale helicopter in ref. [7]. Guo and Chen [8] propose a disturbance-observer-based control (DOBC) method for a particular class of multi-input and multi-output (MIMO) nonlinear systems whose dynamics, such that the disturbance attenuation and rejection problems can be addressed. A nonlinear disturbance observer-based robust control (DOBRC) method is proposed to address the disturbance attenuation problem for nonlinear systems with mismatched disturbances or uncertainties [9]. At the same time, fault tolerant control methods for aircrafts have been studied in, for example refs. [10–13].

*Corresponding author (email: wkjian@126.com)

In order to improve maneuverability, the modeling and control techniques of the morphing aircrafts are studied in some papers. Multi-rigid-body model of the morphing UAV is given in ref. [14]. Under the atmospheric flight condition, the longitudinal and lateral equations are derived in the morphing process. A robust linear control method is adopted to achieve stabilization in maneuvering. The model of morphing UAV is investigated in ref. [15], where an updated camber and span morphing modeling, a parasitic drag modeling, and a dynamic aeroelastic modeling are developed. In ref. [4], a dynamic aeroelastic model is developed, where piezoelectric actuators are used to drive flexible wings and linear quadratic regulation (LQR) method is used for motion control. As reported in ref. [3], computational fluid dynamics can be used to evaluate the morphing wingtip design of a jet, developing the specific models of different flight states. The morphing wing model is established with consideration of the minimum drag of aircraft at different flight speeds, based on which the morphing wing of small-sized UAV is designed [16]. It is revealed that using the morphing wing scheme can improve the aerodynamic performance of the UAV [17]. In ref. [18], the folding wing UAV model is built up, and subsequently an integrated linear parameter varying (LPV) control law is designed. In ref. [19], an aeroservoelastic model of a flexible UAV is built with consideration of model uncertainties, while a robust controller is used to guarantee the stability of the morphing UAV. According to the UAV dynamic response affected by the wing, LPV control method is exploited to enhance the performance [20]. In ref. [21], the aerodynamic model of the morphing wing aircraft is studied. It is interesting to note that aerodynamic force of the morphing UAV can be calculated to change the wing shape, such as sweep, chord length, and thickness. The vortex latice approach can reduce the difficulty of the six-degree of freedom (6DOF) nonlinear dynamics in wing configuration [22]. The mathematical model of variable span UAV is investigated in different wingspan circumstances, and the extra inertial terms are introduced into the moment equations of the 6DOF model in the morphing process [23]. In ref. [24], the time-varying characteristic equations are established when the UAV is morphing, while flight trajectories of the UAV can be tracked well in different sweepback scenarios. The sliding mode control (SMC) method is applied to a morphing UAV, handling the unmodeled dynamics and parametric uncertainties in morphing process [25,26].

To summarize, most of the existing studies have focused on the morphing UAV from the material, structural, and aerodynamic modeling aspects. Nevertheless, the control problem of morphing UAV has not been fully investigated [4,14,18–20,25,26], and rarely consider the anti-disturbance problem. To the best of the authors' knowledge, the anti-disturbance control problem has not been studied for morphing UAVs, which remains an open issue. Motivated by this, we will propose an anti-disturbance control method for the morphing UAV in this paper. The proposed controller has a composite structure which consists of a disturbance observer in the feed-forward channel and a CFBS controller in the feedback channel [6]. Specifically, the idea of DOBC will be borrowed from ref. [8] to deal with the external disturbances, and the CFBS controller will be used to guarantee the stability of the closed loop system while avoiding the phenomenon of differential explosion. It will be shown that, by properly selecting the controller gain, the tracking error is guaranteed to be bounded and the closed-loop system is stable under the proposed composite controller. The main contributions of this paper are presented as follows. First, the inertial forces and inertial moment in the morphing UAV model are treated as bounded disturbances in the control system. Second, the DOs are designed in the morphing process, and the mismatched disturbances are compensated using the CFBS control approach.

The paper is organized as follows. In Sect. 2, the longitudinal dynamics model of a variable sweep UAV is established, and then transformed into a strict feedback form. The control law for the morphing UAV via DO and CFBS methods is designed in Sect. 3, the stability analysis of the control system is given in Sect. 4. Simulation results are given to illustrate the effectiveness of the proposed scheme in Sect. 5. Finally, concluding remarks are drawn in Sect. 6.

2 Morphing UAV model

2.1 Longitudinal dynamics

For the convenience of model establishment, several assumptions are given.

Assumption 1. The morphing UAV is variable-sweep, the wing is rigid body, and the mass of the UAV is constant during flight.

Assumption 2. The morphing UAV is symmetrically constructed, and acceleration of gravity is constant in a low altitude.

Assumption 3. The angle of attack is small in the morphing process and the condition $T\sin\alpha \ll L$ holds. Hence, the term, $T\sin\alpha$, can be ignored in the following.

In terms of the aforementioned assumptions, the longitudinal dynamics of a variable sweep UAV can be written as [14]

$$\begin{aligned}
\dot{V} &= \frac{T\cos\alpha - mg\sin\gamma - D}{m},\\
\dot{h} &= V\sin\gamma,\\
\dot{\gamma} &= \frac{T\sin\alpha + L - mg\cos\gamma - F_{sx}\sin\alpha + F_{sy}\cos\alpha}{mV},\\
\dot{\alpha} &= q - \dot{\gamma},\\
\dot{q} &= \frac{M_{yy} + M_I}{I_{yy}},
\end{aligned} \tag{1}$$

$$\begin{aligned}
F_{sx} &= 2m_1(\ddot{S}_x - q^2 S_x),\\
F_{sy} &= 2m_1(\dot{q}S_x + 2q\dot{S_x}),\\
M_I &= 2m_1 S_x(g\cos\theta + \dot{V}_y + qV_x - \dot{q}S_x - 2q\dot{S_x}),\\
S_x &= a\sin\chi,\\
V_x &= V\cos\alpha\cos\beta,\\
V_y &= -V\sin\alpha\cos\beta,
\end{aligned} \tag{2}$$

where D and L are drag and lift force, respectively. C_L and C_D are denoted as lift coefficient and drag coefficient, respectively. C_{M_q} is moment coefficient due to pitch rate, C_{M_α} is moment coefficient due to angle of attack, and $C_{M_{\delta_e}}$ is moment coefficient due to elevator deflection. I_{yy} is moment of inertial, ρ is the density of air, m_1 is the quality of the single wing, m is the total mass of the UAV, S is reference area of the UAV, $\bar{c}$ is the mean aerodynamic chord, V_x and V_y are the projection on the x axis of the body coordinate and the projection on the y axis of the body coordinate, respectively. β is sideslip angle, a is the constant associated with wing shape, and q is pitch rate.

Remark 1. When the UAV starts morphing, the static moment S_x, which is a function of the sweep angle *chi*, will be included in expressions of the inertial forces and moment (F_{sx}, F_{sy}, M_I). The sweep angle that cannot be accurately given is viewed as the source of parameter uncertainty. Closely dependent on the sweep angle, inertial forces and moment are considered as disturbances in morphing UAV model. The disturbances to be concerned have a great impact on the UAV flight, especially on UAV attitude control.

According to ref. [27], the additional inertial forces F_{sx}, F_{sy} and moment M_I are small when compared to the other forces and moments, which can be regarded as disturbances. Hence, the dynamic model can be greatly simplified. At the same time, the model accuracy will only be affected to a small degree. Moreover, the inertial forces and moment can be estimated as the bounded disturbances in the model. As a result, the equation can be simplified as

$$\dot{V} = \frac{T\cos\alpha - mg\sin\gamma - D}{m}, \tag{3}$$

$$\dot{h} = V\sin\gamma, \tag{4}$$

$$\dot{\gamma} = \frac{T\sin\alpha + L - mg\cos\gamma}{mV} + d_1, \tag{5}$$

$$\dot{\alpha} = q - \dot{\gamma}, \tag{6}$$

$$\dot{q} = \frac{M_{yy}}{I_{yy}} + d_2, \tag{7}$$

where $d_1 = \frac{-F_{sx}\sin\alpha + F_{sy}\cos\alpha}{mV}$ and $d_2 = \frac{M_I}{I_{yy}}$. Notice that d_1 and d_2 can be seen as equivalent bounded disturbances.

It should be mentioned that the state vector and the control input are represented by $X = [V\ h\ \gamma\ \alpha\ q]^{\mathrm{T}}$ and $U = [\delta_T,\ u = \delta_e]$, respectively. The force and moment coefficients are given as [28]

$$C_L = 0.6203\alpha, \tag{8}$$

$$C_D = 0.6450\alpha^2 + 0.0043378\alpha + 0.003772, \tag{9}$$

$$C_T = 0.02576\delta_T, \tag{10}$$

$$C_M(\delta_e) = C_e(\delta_e - \alpha), \tag{11}$$

$$C_{M_\alpha} = -0.035\alpha^2 + 0.036617\alpha + 5.3261\times 10^{-6}, \tag{12}$$

$$C_{M_q} = \frac{\bar{c}}{2V}q(-6.796\alpha^2 + 0.3015\alpha - 0.2289), \tag{13}$$

$$C_e = 0.0292. \tag{14}$$

From the book of the flight control system [29], it is known that

$$\bar{q} = \frac{1}{2}\rho\times V^2, \tag{15}$$

$$T = \bar{q}S\times C_T, \tag{16}$$

$$L = \bar{q}S\times C_L, \tag{17}$$

$$D = \bar{q}S\times C_D, \tag{18}$$

$$M_{yy} = \bar{q}S\,\bar{c}(C_{M_\alpha} + C_{M_{\delta_e}} + C_{M_q}). \tag{19}$$

2.2 System model transformation

Denote $X_1 = [x_1\ x_2\ x_3]^{\mathrm{T}}, x_1 = \gamma, x_2 = \theta, x_3 = q$, and $\theta = \alpha + \gamma$. The dynamics eqs. (5)–(7) can be written in the strict-feedback form. The dynamics equations contain disturbance terms as follows:

$$\begin{aligned}
\dot{x_1} &= f_1(x_1) + g_1(x_1)x_2 + d_1,\\
\dot{x_2} &= f_2(x_1, x_2) + g_2(x_1, x_2)x_3,\\
\dot{x_3} &= f_3(x_1, x_2, x_3) + g_3(x_1, x_2, x_3)u + d_2,\\
y &= x_1,
\end{aligned} \tag{20}$$

where

$$f_1(x_1) = -\frac{g\cos\gamma}{V} - \left(\frac{0.6203\bar{q}S}{mV}\right)\gamma,$$

$$g_1(x_1) = \frac{0.6203\bar{q}S}{mV},$$

$$f_2(x_1, x_2) = 0,\ g_2(x_1, x_2) = 1,$$

$$f_3(x_1, x_2, x_3) = \frac{\bar{q}S\,\bar{c}(C_{M_\alpha} + C_{M_q} - 0.0292\alpha)}{I_{yy}},$$

$g_3(x_1, x_2, x_3) = \dfrac{0.0292\bar{q}S\bar{c}}{I_{yy}}$, and $u = \delta_e$.

In this section, the morphing UAV dynamics model including disturbance is given. The attitude model affected by disturbances is transformed into the strict-feedback form. The composite control law that combines the DO and the CFBS methods will be designed in next section.

3 Controller design

The whole controller consists of two parts, velocity-altitude control via common PID control strategy and attitude control via DO-based CFBS method. The overall anti-disturbance control strategy is depicted in Figure 1.

3.1 Velocity-altitude subsystem control

From eq. (3), the morphing UAV control model can be designed as

$$\begin{cases} \dot{V} = f_V + g_V(\delta_T), \\ \dot{y_V} = V, \end{cases} \tag{21}$$

where $f_V = -\frac{mg\sin\gamma + D}{m}$ and $g_V = 0.01288\rho V^2 S\cos\alpha$. The velocity tracking error can be written as $e_V = V - V_d$, thus one can obtain

$$\dot{e}_V = \dot{V} - \dot{V}_d = f_V + g_V\delta_T - \dot{V}_d. \tag{22}$$

From eq. (22), if control input δ_T can be given as follows:

$$\delta_T = -\frac{f_V + k_V V - k_V V_d - \dot{V}_d}{g_V}, \tag{23}$$

then the control input δ_T can ensure that the velocity tracking error converges to zero. It is noticed that in eq. (23), $k_V > 0$ is the gain of the controller.

Define the tracking error of the altitude as $\tilde{h} = (h - h_d)$. Thus, the flight path command is chosen as

$$\gamma_d = \arcsin\frac{-k_h(h - h_d) - k_I\int(h - h_d)\mathrm{d}t + \dot{h}_d}{V}. \tag{24}$$

Remark 2. $k_h > 0$ and $k_I > 0$ are the gains of the proportion and the integration respectively. If the flight path angle is controlled to follow γ_d, the attitude tracking error is converge to zero exponentially.

3.2 Non-linear disturbance observer design

In general, the non-linear system including disturbances is given as eq. (20), where d_1 and d_2 can be treated as bounded disturbances. For the sake of brevity, f_1 and g_1 are used to replace $f_1(x_1)$ and $g_1(x_1)$, respectively. Eq. (24) can be rewritten as

$$\begin{cases} \dot{x_1} = f_1 + g_1 x_2 + d_1, \\ \dot{x_2} = f_2 + g_2 x_3, \\ \dot{x_3} = f_3 + g_3 u + d_2, \\ y = x_1. \end{cases} \tag{25}$$

Focusing on eq. (25), nonlinear DOs are designed to estimate uncertain disturbances d_1 (mismatched disturbance) and d_2 (matched disturbance) in ref. [30], as follows:

$$\begin{cases} \dot{z_1} = -L_1(\hat{d}_1 + f_1 + g_1 x_2), \\ \hat{d}_1 = z_1 + p_1(x_1), \end{cases} \tag{26}$$

$$\begin{cases} \dot{z_2} = -L_2(\hat{d}_2 + f_3 + g_3 u), \\ \hat{d}_2 = z_2 + p_2(x_3). \end{cases} \tag{27}$$

By letting $\tilde{d}_1 = d_1 - \hat{d}_1$ and $\tilde{d}_2 = d_2 - \hat{d}_2$, the time derivatives of $\tilde{d}_1$ and $\tilde{d}_2$ yield the estimation error dynamics as

$$\dot{\tilde{d}}_1 = \dot{d}_1 - \dot{\hat{d}}_1 = \dot{d}_1 - \dot{z}_1 - L_1\dot{x}_1 = \dot{d}_1 - L_1\tilde{d}_1, \tag{28}$$

$$\dot{\tilde{d}}_2 = \dot{d}_2 - \dot{\hat{d}}_2 = \dot{d}_2 - \dot{z}_2 - L_2\dot{x}_3 = \dot{d}_2 - L_2\tilde{d}_2, \tag{29}$$

where $\hat{d}_1$ and $\hat{d}_2$ are the estimates of unknown disturbances, z_1 and z_2 are the internal states of DOs, $p_1(x_1)$ and $p_2(x_3)$ are non-linear functions to be designed. The gains of DOs $L_1(x_1)$ and $L_2(x_3)$ can be given as

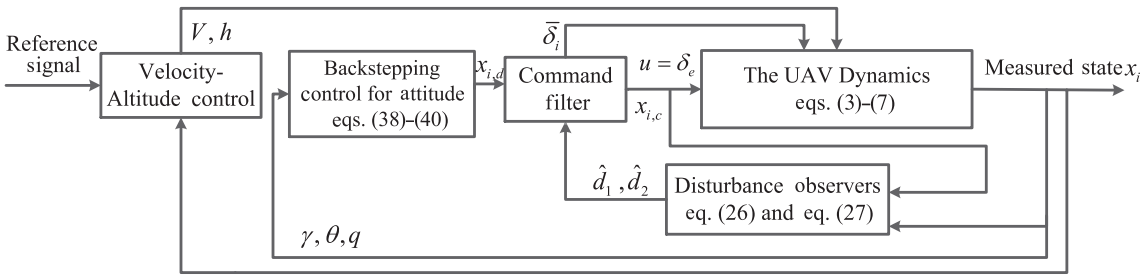

Figure 1 The whole anti-disturbance control strategy.

$$Ł_1(x_1) = \frac{\partial p_1(x_1)}{\partial x_1}, \tag{30}$$

$$Ł_2(x_3) = \frac{\partial p_2(x_3)}{\partial x_3}. \tag{31}$$

In Sect. 4, the convergence of $\tilde{d}_1$ and $\tilde{d}_2$ of the observers will be proved.

3.3 Attitude control via CFBS technique

As is well known, it is difficult for the standard backstepping control methods to solve high order derivation problem, since the derivatives of the virtual control variables may lead to the phenomenon of "differential explosion". By considering this fact, CFBS has been developed in refs. [31,32].

Command filter can be expressed as

$$\begin{bmatrix} \dot{q}_1 \\ \dot{q}_2 \end{bmatrix} = \begin{bmatrix} q_2 \\ 2\zeta\omega_n \left(S_R \left(\frac{\omega_n^2}{2\zeta\omega_n} \left(S_M(x_{i,d}) - q_1 \right) \right) - q_1 \right) \end{bmatrix}, \tag{32}$$

$$\begin{bmatrix} x_{i,c} \\ \dot{x}_{i,c} \end{bmatrix} = \begin{bmatrix} q_1 \\ q_2 \end{bmatrix}. \tag{33}$$

Using command filters, the desired control input $x_{i,d}$ can produce output signal $x_{i,c}$ with upper bounds on amplitude, velocity and bandwidth. The derivatives of $x_{i,c}$ are $\dot{x}_{i,c}$, correspond to the states q_1 and q_2 of command filters respectively. ω_n and ζ correspond to the natural frequency and damping ratio, respectively. $S_M(x)$ and $S_R(x)$ are the functions that provide upper bounds on the amplitude and the rate of the virtual control signal injected to the command filter. Moreover, $S_M(x)$ and $S_R(x)$ can be define as

$$\begin{aligned} S_M(x) &= \begin{cases} M, & \text{if } x \geqslant M, \\ x, & \text{if } |x| < M, \\ -M, & \text{if } x \leqslant -M, \end{cases} \\ S_R(x) &= \begin{cases} R, & \text{if } x \geqslant R, \\ x, & \text{if } |x| < R, \\ -R, & \text{if } x \leqslant -R. \end{cases} \end{aligned} \tag{34}$$

First, $x_{i,c}$ and $\dot{x}_{i,c}$ are generated by the previous stage of virtual control $x_{i,d}$ injected to the command filter. $\delta_i = x_i - x_{i,c}$, $i = 1, 2, 3$ represent the tracking errors. For removing the effect of the command filters, $\bar{\delta}_i$ are the filters unachieved portion of $x_{i,d}$, $\bar{\delta}_i$ are given as follows:

$$\bar{\delta}_i = \delta_i - \xi_i, \tag{35}$$

where $(x_{i,c} - x_{i,d})$ are non-realization part of virtual control signal $x_{i,d}$. ξ_i are dynamic compensation, which can eliminate the influence of non-realization part of virtual control signal. The method can be referred to ref. [28], dynamics of ξ_i are defined as

$$\dot{\xi}_1 = -k_1\xi_1 + g_1(x_{2,c} - x_{2,d}) + g_1\xi_2, \tag{36}$$

$$\dot{\xi}_2 = -k_2\xi_2 + g_2(x_{3,c} - x_{3,d}). \tag{37}$$

By adopting the CFBS algorithm [27], the subsystem can be written as

$$x_{2,d} = \frac{1}{g_1}(-k_1\delta_1 + \dot{x}_{1,c} - f_1 - \hat{d}_1), \tag{38}$$

$$x_{3,d} = \frac{1}{g_2}(-k_2\delta_2 + \dot{x}_{2,c} - f_2 - g_1\bar{\delta}_1), \tag{39}$$

$$u = \frac{1}{g_3}(-k_3\delta_3 + \dot{x}_{3,c} - f_3 - g_2\bar{\delta}_2 - \hat{d}_2), \tag{40}$$

where $k_i > 0$ $(i = 1, 2, 3)$ is control gain, $g_0 = 0$, $x_{1,c} = x_{1,r}$, and $x_{1,r}$, $\dot{x}_{1,r}$ are known, at last, the control input $u = x_{n+1,d}$, $i = 1, 2, 3...n$.

4 Stability analysis

In this section, we will study how to select the controller gains to ensure that the closed-loop system is stable. The stability analysis will be done for the velocity-altitude subsystem in Sect. 4.1 and for the attitude subsystem in Sect. 4.2 respectively.

4.1 Stability analysis of the velocity-altitude control subsystem

For stability analysis of the velocity-altitude control subsystem, the Lyapunov function is chosen as

$$L_{e_V} = \frac{1}{2}{e_V}^2. \tag{41}$$

Differentiating eq. (41) yields

$$\begin{aligned} \dot{L}_{e_V} &= e_V(\dot{e_V}) \\ &= e_V(f_V + g_V\delta_T - \dot{V}_d) \\ &= e_V(f_V - (f_V + k_V V - k_V V_d - \dot{V}_d) - \dot{V}_d) \\ &= e_V(k_V(V_d - V) \\ &= -k_V{e_V}^2, \end{aligned} \tag{42}$$

If $k_V > 0$, then

$$L_{e_V} = -k_V{e_V}^2 \leqslant 0, \tag{43}$$

which guarantees the asymptotic stability of the velocity-altitude subsystem.

4.2 Stability analysis of the attitude control subsystem

The first Lyapunov function of the attitude control subsystem is chosen as

$$V_{L_1} = \frac{1}{2}\bar{\delta_1}^2. \tag{44}$$

Differentiating eq. (44) yields

$$\begin{aligned}\dot{V}_{L_1} &= \bar{\delta}_1(\dot{\bar{\delta}_1})\\ &= \bar{\delta}_1(\dot{\delta}_1 - \dot{\xi}_1)\\ &= \bar{\delta}_1(\dot{x}_1 - \dot{x}_{1,c} - \dot{\xi}_1)\\ &= \bar{\delta}_1(f_1 + g_1x_2 + d_1 - \dot{x}_{1,c} + k_1\xi_1\\ &\quad - g_1(x_{2,c} - x_{2,d}) - g_1\xi_2).\end{aligned} \tag{45}$$

From eqs. (20), (35) and (45), one can achieve

$$\begin{aligned}\dot{V}_{L_1} &= \bar{\delta}_1(f_1 + g_1x_2 + d_1 - \dot{x}_{1,c} + k_1\xi_1 - g_1(x_{2,c} - x_{2,d}) - g_1\xi_2)\\ &= \bar{\delta}_1(f_1 + g_1x_2 + d_1 + k_1\xi_1 - \dot{x}_{1,c} - g_1x_{2,c} - k_1\delta_1\\ &\quad + \dot{x}_{1,c} - f_1 - \hat{d}_1 - g_1\xi_2)\\ &= \bar{\delta}_1(g_1(x_2 - x_{2,c} - \xi_2) + k_1(\xi_1 - \delta_1) + (d_1 - \hat{d}_1))\\ &= \bar{\delta}_1(g_1\bar{\delta}_2 - k_1\bar{\delta}_1 + \tilde{d}_1)\\ &= -k_1\bar{\delta}_1^2 + g_1\bar{\delta}_1\bar{\delta}_2 + \bar{\delta}_1\tilde{d}_1.\end{aligned} \tag{46}$$

Construct the second Lyapunov function as

$$V_{L_2} = V_{L_1} + \frac{1}{2}\bar{\delta_2}^2. \tag{47}$$

By differentiating eq. (47), the derivative of V_{L_2} can be expressed as

$$\begin{aligned}\dot{V}_{L_2} &= \dot{V}_{L_1} + \bar{\delta}_2\dot{\bar{\delta}}_2\\ &= \dot{V}_{L_1} + \bar{\delta}_2(\dot{\delta}_2 - \dot{\xi}_2)\\ &= \dot{V}_{L_1} + \bar{\delta}_2(\dot{x}_2 - \dot{x}_{2,c} - \dot{\xi}_2).\end{aligned} \tag{48}$$

From eqs. (20), (36), (38) and (48), it is yielded that

$$\begin{aligned}\dot{V}_{L_2} &= \dot{V}_{L_1} + \bar{\delta}_2(f_2 + g_2x_3 - \dot{x}_{2,c} + k_2\xi_2 - g_2(x_{3,c} - x_{3,d}))\\ &= -k_1\bar{\delta}_1^2 + g_1\bar{\delta}_1\bar{\delta}_2 + \bar{\delta}_1\tilde{d}_1 + \bar{\delta}_2(f_2 + g_2x_3 - \dot{x}_{2,c}\\ &\quad + k_2\xi_2 - g_2x_{3,c} + g_2x_{3,d})\\ &= -k_1\bar{\delta}_1^2 + g_1\bar{\delta}_1\bar{\delta}_2 + \bar{\delta}_1\tilde{d}_1 + \bar{\delta}_2(g_2(x_3 - x_{3,c})\\ &\quad + k_2(\xi_2 - \delta_2) - g_1\bar{\delta}_1)\\ &= -k_1\bar{\delta}_1^2 + \bar{\delta}_1\tilde{d}_1 + g_2\bar{\delta}_2\delta_3 - k_2\bar{\delta}_2^2\\ &= -k_1\bar{\delta}_1^2 - k_2\bar{\delta}_2^2 + g_2\bar{\delta}_2\delta_3 + \bar{\delta}_1\tilde{d}_1.\end{aligned} \tag{49}$$

The third Lyapunov function is chosen as

$$V_{L_3} = V_{L_2} + \frac{1}{2}\delta_3^2. \tag{50}$$

By differentiating eq. (50), the derivative of V_{L_3} can be expressed as

$$\dot{V}_{L_3} = \dot{V}_{L_2} + \delta_3\dot{\delta}_3 = \dot{V}_{L_2} + \delta_3(\dot{x}_3 - \dot{x}_{3,c}). \tag{51}$$

From eqs. (20), (39) and (51), we have

$$\begin{aligned}\dot{V}_{L_3} &= \dot{V}_{L_2} + \delta_3(f_3 + g_3u + d_2 - \dot{x}_{3,c})\\ &= \dot{V}_{L_2} + \delta_3(f_3 - k_3\delta_3 + \dot{x}_{3,c} - f_3 - g_2\bar{\delta}_2 - \hat{d}_2 + d_2 - \dot{x}_{3,c})\\ &= -k_1\bar{\delta}_1^2 - k_2\bar{\delta}_2^2 + g_2\bar{\delta}_2\delta_3 + \bar{\delta}_1\tilde{d}_1\\ &\quad + \delta_3(-k_3\delta_3 - g_2\delta_2 + \tilde{d}_2)\\ &= -k_1\bar{\delta}_1^2 - k_2\bar{\delta}_2^2 - k_3\delta_3^2 + \bar{\delta}_1\tilde{d}_1 + \delta_3\tilde{d}_2.\end{aligned} \tag{52}$$

To analyze the dynamic errors, the fourth Lyapunov function is defined as

$$V_{L_4} = V_{L_3} + \frac{1}{2}\tilde{d}_1^2 + \frac{1}{2}\tilde{d}_2^2. \tag{53}$$

By differentiating eq. (53), the derivative of V_{L_4} can be represented as

$$\dot{V}_{L_4} = \dot{V}_{L_3} + \tilde{d}_1\dot{\tilde{d}}_1 + \tilde{d}_2\dot{\tilde{d}}_2. \tag{54}$$

Substituting eqs. (28) and (29) into eq. (54) can render

$$\begin{aligned}\dot{V}_{L_4} &= \dot{V}_{L_3} + \tilde{d}_1(-L_1\tilde{d}_1 + \dot{d}_1) + \tilde{d}_2(-L_2\tilde{d}_2 + \dot{d}_2)\\ &= -k_1\bar{\delta}_1^2 - k_2\bar{\delta}_2^2 - k_3\delta_3^2 + \bar{\delta}_1\tilde{d}_1 + \delta_3\tilde{d}_2 - L_1\tilde{d}_1^2\\ &\quad + \tilde{d}_1\dot{d}_1 - L_2\tilde{d}_2^2 + \tilde{d}_2\dot{d}_2\\ &\leqslant -\left(k_1 - \frac{1}{2}\right)\bar{\delta}_1^2 - k_2\bar{\delta}_2^2 - \left(k_3 - \frac{1}{2}\right)\delta_3^2\\ &\quad - \left(L_1 - \frac{1}{2}\right)\tilde{d}_1^2 - \left(L_2 - \frac{1}{2}\right)\tilde{d}_2^2 + \tilde{d}_1\dot{d}_1 + \tilde{d}_2\dot{d}_2.\end{aligned} \tag{55}$$

By letting $L_1 = l_1 + \frac{1}{2}$, $L_2 = l_2 + \frac{1}{2}$, $l_1 > 0$, and $l_2 > 0$, one can have

$$\begin{aligned}\dot{V}_{L_4} &\leqslant -\left(k_1 - \frac{1}{2}\right)\bar{\delta}_1^2 - k_2\bar{\delta}_2^2 - \left(k_3 - \frac{1}{2}\right)\delta_3^2\\ &\quad - l_1\tilde{d}_1^2 - l_2\tilde{d}_2^2 + \tilde{d}_1\dot{d}_1 + \tilde{d}_2\dot{d}_2\\ &\leqslant -\left(k_1 - \frac{1}{2}\right)\bar{\delta}_1^2 - k_2\bar{\delta}_2^2 - \left(k_3 - \frac{1}{2}\right)\delta_3^2\\ &\quad - l_1\tilde{d}_1^2 - l_2\tilde{d}_2^2 + |\tilde{d}_1||\dot{d}_1| + |\tilde{d}_2||\dot{d}_2|.\end{aligned} \tag{56}$$

Focusing on

$$-l_1\tilde{d}_1^2 + |\tilde{d}_1||\dot{d}_1| = |\tilde{d}_1|(-l_1|\tilde{d}_1| + |\dot{d}_1|), \tag{57}$$

if $|\tilde{d}_1| \geqslant \frac{1}{l_1}|\dot{d}_1|$, then

$$|\tilde{d}_1|(-l_1|\tilde{d}_1| + |\dot{d}_1|) \leqslant 0. \tag{58}$$

Similarly, if $|\tilde{d}_2| \geqslant \frac{1}{l_2}|\dot{d}_2|$, the following condition holds:

$$|\tilde{d}_2|(-l_2|\tilde{d}_2| + |\dot{d}_2|) \leqslant 0, \tag{59}$$

where $|\dot{d}_1| \leqslant \bar{d}_1$ and $|\dot{d}_2| \leqslant \bar{d}_2$, in other words, if $|\tilde{d}_1|(-l_1|\tilde{d}_1| + |\dot{d}_1|) \leqslant 0$, $|\tilde{d}_2|(-l_2|\tilde{d}_2| + |\dot{d}_2|) \leqslant 0$, can get the conclusion

$$\dot{V}_{L_4} \leqslant -\left(k_1 - \frac{1}{2}\right)\bar{\delta}_1^{\,2} - k_2\bar{\delta}_2^{\,2} - \left(k_3 - \frac{1}{2}\right)\delta_3^{\,2} - \left(L_1 - \frac{1}{2}\right)\tilde{d}_1^{\,2} - \left(L_2 - \frac{1}{2}\right)\tilde{d}_2^{\,2}. \tag{60}$$

From the expressions of the d_1 and d_2, the boundary of the disturbances can be obtained. In fact, the maneuverability of the morphing UAV is limited in morphing process, hence the change rates of the disturbances $\dot{d}_1$ and $\dot{d}_2$ are bounded. In summary, the conditions $|\dot{d}_1| \leqslant \bar{d}_1$ and $|\dot{d}_2| \leqslant \bar{d}_2$ hold, leading to

$$|\tilde{d}_1| \leqslant \frac{1}{l_1}|\bar{d}_1| \leqslant \frac{1}{l_1}|\dot{d}_1|. \tag{61}$$

Therefore, the closed-loop system is input-to-state stable (ISS), which implies that the system states and the estimation errors are bounded.

5 Numerical simulation

5.1 Simulation scenario

In the simulation, the UAV starts the morphing process at 8 s, the whole morphing phase is over at 50 s. The longitudinal dynamics of the UAV are involved in simulation studies due to the fact that disturbances mainly affect longitudinal attitude in the morphing process. At the same time, the velocity of the UAV can keep stable. The inertial forces and moment are slow-varying during the morphing process.

(1) The UAV initial condition

It is assumed that the initial flight altitude of the UAV is $h_0 = 110000$ ft and flight speed is $V_0 = 15060$ ft/s. The air density of the desired altitude is $\rho = 2.4325 \times 10^{-5}$ slug/ft^3, and the mass of the UAV is given as m=9375 slug (1 slug is approximately equal to 14.594 kg).

(2) The gains of DO and control

The first DO gain is $l_1 = 100$, The second DO gain is $l_2 = 100$; and the gain of flight speed control is $k_V = 1$. The parameters of altitude control including the gain of the proportion and the gain of the integration is is given by $k_h = 0.4$ and $k_I = 0.5$ respectively in simulation. The CFBS controller gains are $k_1 = 1$, $k_2 = 2$, and $k_3 = 3$ respectively.

(3) The simulation condition

The desired tracking altitude is $h_d = 115000$ ft, the desired flight velocity increment is $v = 100$ ft/s, the inertia moment of the UAV is $I_{yy} = 7 \times 10^6$ slug ft^2. The sideslip angle is $\beta = 0°$ in the morphing phase, the mean aerodynamic chord is $\bar{c} = 80$ ft, and the reference area of the UAV is $S = 3603$ ft^2.

The elevator is described as a two order dynamic system. The simulation parameters are selected as follows in Table 1. The simulation lasts 50 s which contains the whole process of the morphing.

5.2 Results analysis

Figure 2 indicates that the flight velocity of the UAV can converge to the desired flight speed 15160 ft/s from the beginning velocity 15060 ft/s. The UAV can reach to the expected altitude of 115000 ft. The simulation indicates that the morphing UAV can keep at 115000 ft altitude as shown in Figure 2.

The disturbances are related to the inertial forces and inertial moment. The disturbances can be well estimated. The curves of the disturbances and the disturbance estimations are shown in Figure 3. It is clear that the estimated value and actual value are close.

The morphing UAV will fly from the initial altitude to the desired altitude. The flight path angle can quickly track the desired flight path angle as shown in Figure 4(a), even though

Table 1 The parameters of the command filters

The number of the command filters	Natural frequency	Damping ratio
CF_1	$w_1 = 80$	$\zeta_1 = 0.7$
CF_2	$w_2 = 180$	$\zeta_2 = 0.7$
CF_3	$w_3 = 200$	$\zeta_3 = 0.7$

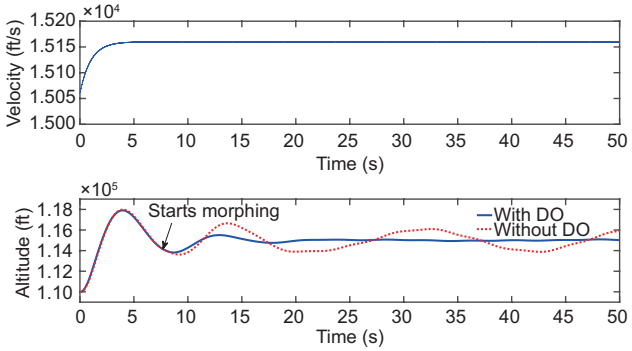

Figure 2 (Color online) Flight velocity and altitude in the morphing process.

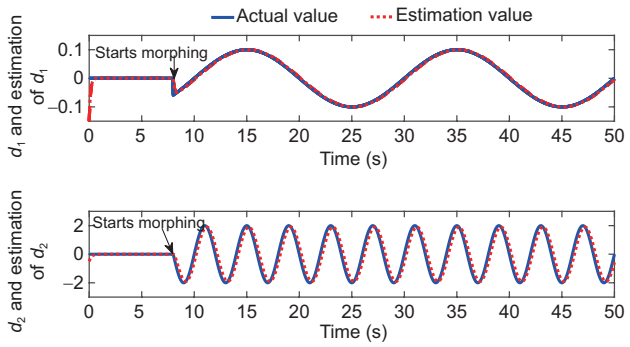

Figure 3 (Color online) Disturbance and estimation of disturbance.

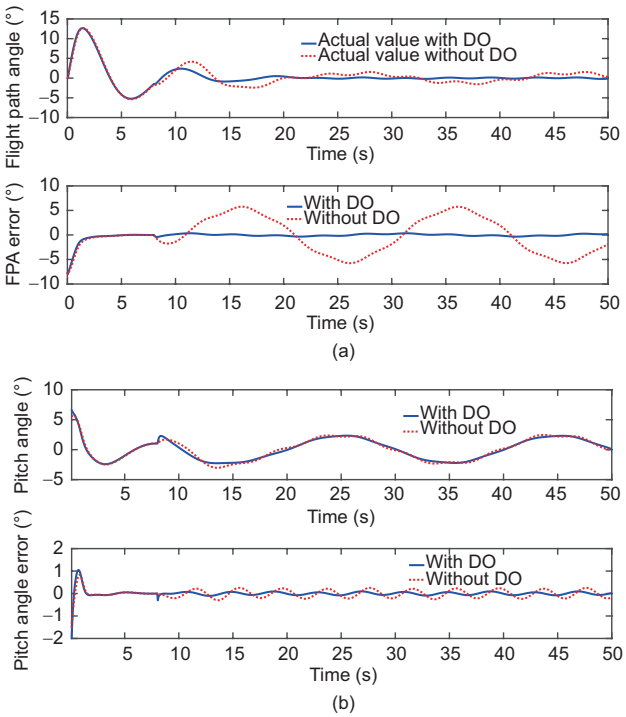

Figure 4 (Color online) Angle comparison curve. (a) Flight path angle; (b) pitch angle.

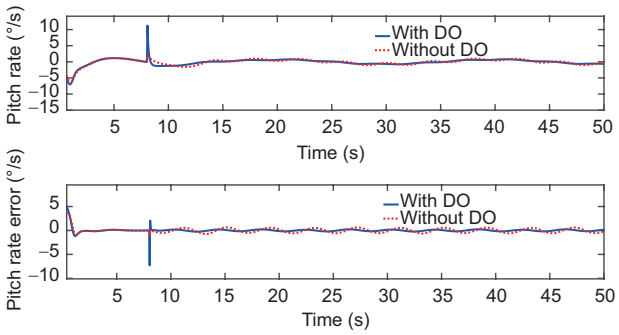

Figure 5 (Color online) Pitch rate.

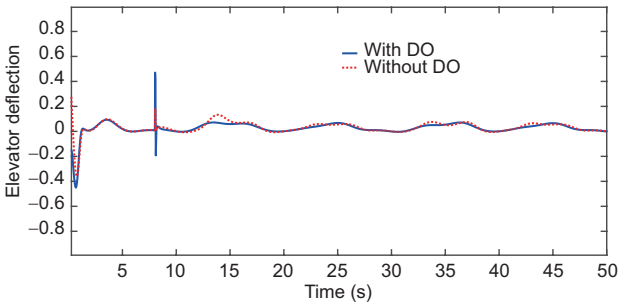

Figure 6 (Color online) Elevator deflection.

the UAV starts morphing at 8 s. As can be seen from Figures 4(b) and 5, the pitch angle and pitch rate converge to the neighborhood of zero quickly. The elevator deflection shown in Figure 6 is designed to control the flight-path angle. It can be observed that the elevator deflection can converge to the steady state quickly.

The curve of the flight path angle rate in Figure 5 shows that the UAV can move at a relatively stable speed from the 10th second. The results presented in Figures 4 and 5 confirm that, under the DO-CFBS approach, the path angle tracking errors, the pitch angle tracking errors, and the pitch rate tracking error can converge to zero within a finite time.

From the results shown in Figures 3–5, the DO-CFBS control method achieves enhanced stability than the conventional CFBS method. Under the proposed anti-disturbance method, the tracking errors of pitch rate converge to their steady state values more quickly. Hence, the tracking performance achieved by the proposed control scheme is better than that under the control without any DOs.

From above the simulations, we can conclude that the UAV is more stable in desired flight path angle, through the disturbance-observer-based CFBS control method when comparing to the CFBS control method. The contrast curves of the system are given including the flight path angle, the pitch angle and pitch angle rate with DO and without DO. It is clear that the disturbances of the morphing UAV can be estimated and rejected. It can also be observed that the DO-CFBS control method can improve the robustness and anti-disturbance performance of the system.

To further illustrate the effectiveness of the proposed anti-disturbance approach, the root mean squared error (RMSE) is defined as

$$\mathrm{RMSE}_i := \sqrt{\frac{1}{N}\sum_{n=1}^{N} e_i^2(n)}, \tag{62}$$

where $e_i(n)$ denotes the steady state error of the ith error term at time n. The obtained data are presented in Table 2.

The prescribed performance indices exemplify that the DO-CFBS method has outperformed the conventional CFBS in terms of RMSE.

6 Conclusion

This paper proposes a novel control method for the morphing UAV via CFBS method and DO technique. It can be shown

Table 2 RMSEs with and without DO

	RMSE without DO	RMSE with DO	Improved rates
Altitude	789.702	155.029	80.37%
Flight path angle	4.417	1.342	69.62%
Pitch angle	0.167	0.020	88.02%
Pitch rate	0.305	0.179	41.31%

that the system outputs can track the reference signals when the DO-CFBS control scheme is applied. The presented control method has the following advantages: the proposed control strategy can not only enhance disturbance rejection performance and robustness but also improve system anti-disturbance capability. The simulation results show that the DO-CFBS scheme can achieve better tracking performance and robustness than the schemes without DO. This paper provides a feasible solution to the complex control problem for the morphing UAV.

1 Weisshaar T. Morphing Aircraft Technology-New Shapes for Aircraft Design. NATO Report. NATO-MP-AVT-141, Aeronautical Science and Technology, 2006
2 Weisshaar T. Morphing aircraft systems: Historical perspectives and future challenges. J Aircraft, 2015, 99: 337–353
3 Cooper J E, Chekkal I, Cheung RCM, et al. Design of a morphing-wingtip. J Aircraft, 2015, 52: 1–8
4 Tsushima N, Su W. Active piezoelectric actuation and control of highly flexible multifunctional wings. In: Proceedings of the AIAA/ASCE/AHS/ASC Structures, Structural Dynamics, and Materials Conference. California, 2016. 0715
5 Albuquerque P F, Gamboa P V, Silvestre M. Multidisciplinary and multilevel aircraft design methodology using enhanced collaborative optimization. In: Proceedings of the AIAA/ISSMO Multidisciplinary Analysis and Optimization Conference. Dallas, 2015. 2650
6 Lu H, Wang N, Qiao J, et al. Nolinear disturbance observer based command filtered backstepping control for missile system. In: Proceedings of the 32nd Chinese Control Conference. Xi'an, 2013. 4311–4316
7 Lu H, Liu C, Guo L, et al. Flight control design for small-scale helicopter using disturbance-observer-based backstepping. J Guidance Control Dyn, 2015, 38: 2235–2240
8 Guo L, Chen W H. Disturbance attenuation and rejection for systems with nonlinearity via DOBC approach. Int J Robust Nonlinear Control, 2005, 15: 109–125
9 Chen W H, Li S, Yang J. Non-linear disturbance observer-based robust control for systems with mismatched disturbances/uncertainties. IET Control Theor Appl, 2011, 5: 2053–2062
10 Yu X, Fu Y, Li P, et al. Fault-tolerant aircraft control based on self-constructing fuzzy neural networks and multivariable SMC under actuator faults. IEEE Trans Fuzzy Syst, 2018, 26: 2324–2335
11 Yu X, Li P, Zhang Y. The design of fixed-time observer and finite-time fault-tolerant control for hypersonic gliding vehicles. IEEE Trans Ind Electron, 2018, 65: 4135–4144
12 Yu X, Fu Y, Zhang Y. Aircraft fault accommodation with consideration of actuator control authority and gyro availability. IEEE Trans Contr Syst Technol, 2018, 26: 1285–1299
13 Yu X, Liu Z, Zhang Y. Fault-tolerant flight control design with finite-time adaptation under actuator stuck failures. IEEE Trans Contr Syst Technol, 2017, 25: 1431–1440
14 Seigler T M. Dynamics and Control of Morphing Aircraft. Dissertation for Dcotoral Degree. Blacksburg: Virginia Polytechnic Institude and State University, 2005
15 Werter N, Breuker R D. A framework for the aeroelastic analysis and design of generic morphing wings. In: Proceedings of the 23rd AIAA/AHS Adaptive Structures Conference. Kissimmee, 2015. 5–9
16 Vale J, Lau F, Suleman A, et al. Multidisciplinary design optimization of a morphing wing for an experimental UAV. In: Proceedings of the 11th AIAA/ISSMO Multidisciplinary Analysis and Optimization Conference. Portsmouth, 2006. 1–10
17 Oliviu S G, Koreanschi A, Bote R M. Numerical study of UAS-S4 hecatl aerodynamic performance improvement obtained with the use of a morphing wing approach. In: Proceedings of the AIAA Aviation 2015, AIAA Applied Aerodynamics Conference. Dallas, 2015. 2259
18 Yue T, Wang L, Ai J. Longitudinal integrated linear parameter varying control for morphing aircraft in large flight envelope. In: Proceedings of the AIAA Atmospheric Flight Mechanics Conference. Denver, 2017. 3396
19 Kotikalpudi A, Pfifer H, Seiler P. Sensitivity of robust flutter boundary to model uncertainties in aeroservoelastic systems. In: Proceedings of the AIAA Atmospheric Flight Mechanics Conference. Kissimmee, 2015. 1752
20 Baldelli D H, Lee D H, Sánchez Peña R S, et al. Modeling and control of an aeroelastic morphing vehicle. J Guidance Control Dyn, 2008, 31: 1687–1699
21 Niksch A, Valasek J, Strganac T, et al. Six degree of freedom dynamical model of a morphing aircraft. In: Proceedings of the The AIAA Atmospheric Flight Mechanics Conference. Chicago, 2009. 5849: 10–13
22 Obradovic B, Subbarao K. Modeling of flight dynamics of morphing wing aircraft. J Aircraft, 2011, 48: 391–402
23 Henry J, Pines D. A mathematical model for roll dynamics by use of a morphing-span wing. In: Proceedings of the AIAA/ASME/ASCE/AHS/ASC Structures, Structural Dynamics, and Materials Conference. Honolulu, 2007. 1708
24 Chakravarthy A, Grant D, Lind R. Time-varying dynamics of a micro air vehicle with variable-sweep morphing. J Guidance Control Dyn, 2012, 35: 890–903
25 Yin M, Lu Y P, He Z, et al. Modeling and sliding mode control of morphing aircraft for morphing-aided maneuver. Syst Eng Electron, 2015, 37: 128–134
26 Wang L, Su J. Disturbance rejection control of a morphing UAV. In: Proceedings of the American Control Conference. Washington, 2013. 4307–4312
27 Seigler T M, Neal D A, Bae J S, et al. Modeling and flight control of large-scale morphing aircraft. J Aircraft, 2007, 44: 1077–1087
28 Xu H, Mirmirani M D, Ioannou P A. Adaptive sliding mode control design for a hypersonic flight vehicle. J Guidance Control Dyn, 2004, 27: 829–838
29 Etkin B, Lloyd D R. Dynamics of Flight: Stability and Control. New York: Wiley, 1996. 51–80
30 Chen W H. Nonlinear disturbance observer-enhanced dynamic inversion control of missiles. J Guidance Control Dyn, 2003, 26: 161–166
31 Farrell J, Sharma M, Polycarpou M. Backstepping-based flight control with adaptive function approximation. J Guidance Control Dyn, 2005, 28: 1089–1102
32 Farrell J A, Polycarpou M, Sharma M, et al. Command filtered backstepping. IEEE Trans Automat Contr, 2009, 54: 1391–1395